Raman Spectroscopic and *ab initio* Quantum Chemical Investigations of Molecules and Complex Ions in the Molten System $CsCl-NbCl_5-NbOCl_3$

Christian Rosenkilde, George Voyiatzis,† Vidar R. Jensen, Martin Ystenes, and Terje Østvold*

Institute of Inorganic Chemistry, Norwegian Institute of Technology (NTH), N-7034 Trondheim, Norway, and Institute of Chemical Engineering and High Temperature Chemical Processes (ICE/HT), P.O. Box 1414 GR-26500 Patras, Greece

Received August 24, 1994®

Raman spectroscopy has been used to study the liquid system $CsCl-NbCl_5-NbOCl_3$ at temperatures between 340 and 650 °C. Molten $NbOCl_3$ shows Raman bands typical of bridging and terminal oxygen. In the basic regions of the system the ions $NbCl_6^-$, $NbOCl_5^{2-}$, and $NbOCl_4^-$ have been identified. In the acidic region, polymeric ions with bridging oxygen probably coexist with ions with terminal oxygen. The structure of $NbCl_6^-$, $NbOCl_5^{2-}$, and $NbOCl_4^-$ have been verified by and the interpretation of their spectra assisted with *ab initio* SCF and CASSCF calculations. SCF calculations have also been performed for $NbCl_5$ and $NbOCl_3$, and $VOCl_3$, $VOCl_4^-$, and $VOCl_5^{2-}$ for comparison. In the binary $CsCl-NbOCl_3$, when $x_{CsCl} > 0.5$, the equilibrium $NbOCl_4^- + Cl^- = NbOCl_5^{2-}$ is established. This is also verified by quantum chemical calculations.

Introduction

There has been an increasing interest in the chemistry of niobium in molten salts in the last years. This is linked to their potential as electrolytes for electrodeposition of niobium.[1] The chemistry of niobium in alkali chloride melts is interesting in this context. As a part of a study on the chemistry of niobium chlorides and oxochlorides[2-5] in molten alkali chloride melts, we have investigated molecules and ions in the molten system $CsCl-NbCl_5-NbOCl_3$ by Raman spectroscopy and *ab initio* quantum chemical calculations. The system is a part of the reciprocal ternary system $Cs_2O-CsCl-NbCl_5-Nb_2O_5$. The binaries in the system, $CsCl-NbCl_5-NbOCl_3$, $CsCl-NbCl_5$, $CsCl-NbOCl_3$, and $NbCl_5-NbOCl_3$, have been fairly well studied by thermal analysis.[6-10] Some IR and Raman spectroscopic investigations have also been reported for the first two systems,[11-16] but for the ternary system, which is the subject of the present work, the amount of data available in the literature is scarce.

In the system $NbCl_5-CsCl$ one binary compound, $CsNbCl_6$, is reported,[6] and Raman spectroscopic evidence of the octahedral ion $NbCl_6^-$ in the melt has been given.[11,12] Raman spectra of molten $NbCl_5$ have been recorded[11,17] and show that the melt consists of monomeric $NbCl_5$ and dimeric Nb_2Cl_{10}. Spectra of the solid show only bands belonging to the dimer,[11,18] while gas phase Raman spectra indicate that gaseous $NbCl_5$ is monomeric.[11,19]

There are some disagreements as to the numbers of solid compounds formed in the system $NbOCl_3-CsCl$. In one paper it is claimed that Cs_2NbOCl_5 and $CsNbOCl_4$ are the only two compounds,[7] while another paper presents evidence for a third compound, Cs_3NbOCl_6.[8] Raman spectroscopic studies are reported for both solid and gaseous $NbOCl_3$,[13] solid $PPh_3Me[NbOCl_4(CH_3CN)]$,[20] and $[As(C_6H_5)_4]_2NbOCl_5$ dissolved in CH_2Cl_2.[21] IR spectra are reported for solid Cs_2NbOCl_5,[14-16] $(C_5H_5NH)NbOCl_4$,[22] $PPh_3Me[NbOCl_4(CH_3CN)]$,[20] and $(C_9H_7NH)NbOCl_4$.[22] Both dissolved and solid $NbOCl_5^{2-}$ show a band at approximately 920 cm^{-1} which is assigned to the Nb=O stretching mode. Hiller and Strähle[20] give the same assignment to the band at 960 cm^{-1} for $NbOCl_4^-$. Gaseous $NbOCl_3$ has a band at 993 cm^{-1}, which also is assigned to the Nb=O stretch. Solid $NbOCl_3$, $(C_5H_5NH)NbOCl_4$, and $(C_9H_7NH)NbOCl_4$ show bands respectively at 770, 850, and 800 cm^{-1}, which are attributed to oxygen bridging, i.e., Nb–O–Nb. Binary compounds have not been found in the system $NbCl_5-NbOCl_3$.[9] When heated at low pressures, $NbOCl_3$ partly disproportionates to $NbCl_5$ and Nb_2O_5. This disproportionation is greatly reduced by the presence of molten $NbCl_5$.[9,23]

In the ternary system $CsCl-NbOCl_3-NbCl_5$, the compound $CsNb_2OCl_9$ has been prepared from $NbOCl_3$ and $CsNbCl_6$.[10]

* Author to whom correspondence should be addressed at the Norwegian Institute of Technology.
† ICE/HT.
® Abstract published in *Advance ACS Abstracts,* July 15, 1995.

(1) Mellors, G. W.; Senderoff, S. *J. Electrochem. Soc.* **1965**, *112*, 266.
(2) Bachtler, M.; Rockenberger, J.; Freyland, W.; Rosenkilde, C.; Østvold, T. *J. Phys. Chem.* **1994**, *98*, 742.
(3) Rosenkilde, C.; Østvold, T. *Acta Chem. Scand.* **1994**, *48*, 732.
(4) Rosenkilde, C.; Østvold, T. *Acta Chem. Scand.* **1995**, *49*, 85.
(5) Rosenkilde, C.; Østvold, T. *Acta Chem. Scand.* **1995**, *49*, 265.
(6) Huber, K.; Jost, E. *Helv. Chim. Acta* **1958**, *41*, 2411.
(7) Morozov, S.; Krokhin, V. A. *Russ. J. Inorg. Chem. (Engl. Transl.)* **1963**, *8*, 1245.
(8) Shchukarev, S. A.; Smirnova, E. K.; Vasil'kova, I. V. *Vestn. Leningr. Univ. Ser. Fiz. Khim.* **1963**, *16*, 132.
(9) Nisel'son, L. A.; Gavrilov, O. R. *Russ. J. Inorg. Chem. (Engl. Transl.)* **1967**, *12*, 1674.
(10) Churikova, M. B.; Smirnova, E. K.; Vasil'kova, I. V. *Russ. J. Inorg. Chem. (Engl. Transl.)* **1971**, *16*, 290.
(11) Bues, W.; Demiray, F.; Øye, H. A. *Z. Phys. Chem., Neue Folge* **1973**, *84*, 18.
(12) Kipouros, G. J.; Flint, J. H.; Sadoway, D. R. *Inorg. Chem.* **1985**, *24*, 3881.
(13) Beattie, I. R.; Livingstone, K. M. S.; Reynolds, D. J.; Ozin, G. A. *J. Chem. Soc. A* **1970**, 1210.
(14) Wendling, E.; Rohmer, R. *Bull. Soc. Chim. Fr.* **1967**, *1*, 8.
(15) Sabatini, A.; Bertini, I. *Inorg. Chem.* **1966**, *5*, 204.
(16) Brown, D. *J. Chem. Soc. A* **1964**, 4944.
(17) Krebs, B.; Janssen, H.; Bjerrum, N. J.; Berg, R. W.; Papatheodorou, G. N. *Inorg. Chem.* **1984**, *23*, 164.
(18) Beattie, I. R.; Gilson, T. R.; Ozin, G. A. *J. Chem. Soc. A* **1968**, 2765.
(19) Beattie, I. R.; Ozin, G. A. *J. Chem. Soc. A* **1969**, 1691.
(20) Hiller, W.; Strähle, J.; Prinz, H.; Dehnicke, K. *Z. Naturforsch.* **1984**, *39B*, 107.
(21) Müller, U.; Lorentz, I. *Z. Anorg. Allg. Chem.* **1980**, *463*, 110.
(22) Morozov, S.; Lipatova, N. P. *Russ. J. Inorg. Chem. (Engl. Transl.)* **1968**, *13*, 1101.
(23) Meyer, G.; Oosterom, J. F.; Van Oeveren, W. J. *Trav. Chim. Pays-Bas* **1961**, *80*, 502.

0020-1669/95/1334-4360$09.00/0

Table 1. Wavenumbers of Important Vibrational Frequencies for Different Nb–Chlorides and Nb–Oxochlorides and Related Compounds[a]

compound	Nb–X breath	Nb=O stretch	Nb–O–Nb sym. stretch	other	method	ref
$NbCl_5(g)$	394			316	Raman	11, 19
$NbCl_5(s)$	397				Raman	11, 18
$NbCl_6^-$	373				Raman	11, 12
$NbOCl_3(g)$	395	997			Raman	13
$NbOCl_3(s)$	421		770		Raman	13
$NbOCl_3(s)$			767		IR	16
$PPh_3Me[NbOCl_4(CH_3CN)]$	333	960		312	Raman	20
$PPh_3Me[NbOCl_4(CH_3CN)]$		956		315	IR	20
$(C_5H_5NH)NbOCl_4$			850		IR	22
$C_9H_7NH)NbOCl_4$			800		IR	22
$[As(C_6H_5)_4]_2NbOCl_5$	340	923		241	Raman	21
$Cs_2NbOCl_5(s)$		922		325	IR	14
$Cs_2NbOCl_5(s)$		922		319	IR	16
$NbF_n^{(n-5)-}$	626			371, 290	Raman	25
$NbOF_n^{(n-3)-}$	583	921		307, 266	Raman	25
$NbO_2F_x^{(x-1)-}$		878		815, 360	Raman	25
$VOCl_3(g)$	408	1042		125	Raman	13
$VOCl_3(l)$	411.5	1037.5		132	Raman	27
$[Cl_3PNPCl_3][VOCl_4]$		1023		165	IR	28

[a] Wavenumbers in cm^{-1} in this and the other tables.

Table 2. Nominal Compositions of the Mixtures Studied in this Work (Concentrations in mol %)

sample	CsCl	$NbOCl_3$	$NbCl_5$	description	spectra in figure
I	0	0	100	$NbCl_5$	
II	0	100	0	$NbOCl_3$	3
III	50	50	0	$CsNbOCl_4$	4
IV	60	40	0	$Cs_2NbOCl_5 + CsNbOCl_4$	4
V	66.6	33.3	0	Cs_2NbOCl_5	4
VI	80	20	0	$Cs_2NbOCl_5 + 2CsCl$	4
VII	95	5	0	$Cs_2NbOCl_5 + 17CsCl$	4
VIII	50	0	50	$CsNbCl_6$	2
IX	33.3	33.3	33.3	$CsNb_2OCl_9$	6
X	40	20	40	$CsNbCl_6 + CsNb_2OCl_9$	7
XI	40	40	20	$CsNbOCl_4 + CsNb_2OCl_9$	6
XII	50	25	25	$CsNbOCl_4 + CsNbCl_6$	5

The same authors also prepared KNb_2OCl_9. Thermal analyses have been performed in the systems $KNbCl_6$–$NbOCl_3$, $KNbOCl_4$–$NbCl_5$, and $KNbOCl_4$–$KNbCl_6$.[24] Liquidus data for the system $NbOCl_3$–$KNbCl_6$ suggest formation of KNb_2OCl_9.

Niobium oxofluorides have also been studied by Raman spectroscopy. von Barner *et al.*[25] found $NbF_n^{(n-5)-}$, $NbOF_x^{(x-3)-}$ and $NbO_2F_y^{(y-1)-}$ when 2.7 mol % K_2NbF_7 was added to a molten mixture of LiF, NaF, and KF with different oxide concentrations.

Both Raman and IR spectra have been recorded of vanadium oxochlorides. Raman spectra of $VOCl_3$ in both the vapor and the solid state show bands belonging to monomeric molecules with C_{3v} symmetry,[13,26] as is also found for liquid $VOCl_3$.[27] IR spectra have been recorded of $[Cl_3PNPCl_3][VOCl_4]$[28] and no sign of bridging oxygen atoms were found. A summary of vibrational frequencies for species of interest to the present work is given in Table 1.

Apart from a geometry calculation for $MoCl_5$[29] and electronic structure determinations for $VOCl_3$ and $NbOCl_3$,[30] no *ab initio* quantum chemical calculations for niobium chlorides or related species have been found in the literature. Quantum chemical vibrational analysis on transition metal chlorides have been reported for $TiCl_4$[31] and Zn^{2+} [32,33] species. Although they both handle first row transition elements, they indicate that SCF calculations should work well when near degeneracy effects are not important.

In the present work, quantum chemical calculations have been included partly to establish an independent basis for the assignment of the vibrational spectra of the species, and partly to verify the symmetry of the ions. However, such structure determinations sometimes end up with inaccurate, and even erroneous, results, especially for charged species. Independent verification of the results is therefore crucial, and a second objective of the quantum chemical vibrational analysis is to achieve testable predictions from the geometry calculations. This principle of using quantum chemistry to predict a molecular geometry and verify the result by comparing experimental and theoretical vibrational spectra is well established in the literature, although to a lesser extent for inorganic species.[34,35,36] To establish a sound basis for our conclusions we have included in our calculations niobium chloride and oxochloride species and the homologous vanadium oxochloride species. We have also evaluated theoretically an equilibrium found in the CsCl–$NbOCl_3$ system.

Experimental Section

All samples (typically 300 mg) were prepared by mixing $NbCl_5$ (Alfa grade 1), Nb_2O_5 (Alfa, 99.9%, dried at 200 °C at 10^{-3} mbar) and CsCl (Fluka, 99.9%, melt bubbled with dry HCl and finally recrystallized) in a quartz cell (o.d. 4 × 2 mm). All handling of the salts was performed in a drybox with water and oxygen levels below 1 ppm. The filled cell was sealed off on a vacuum line ($<10^{-2}$ mbar). Salts melting at temperatures below 650 °C were melted and mixed and kept in the molten state until all of the $Nb_2O_5(s)$ was dissolved. The melting and mixing procedure was done carefully due to high vapor pressures of $NbCl_5$ (bp 250 °C), and for the same reasons, the volume above the

(24) Niels'son, L. A.; Gavrilov, O. R. *Zh. Prikl. Chim.* **1967**, *15*, 762.
(25) vonBarner, J. H.; Christensen, E.; Bjerrum, N. J.; Gilbert, B. *Inorg. Chem.* **1991**, *30*, 561.
(26) Clark, R. J. H.; Mitchell, P. D. *J. Chem. Soc., Dalton Trans.* **1972**, *22*, 2429.
(27) Demiray, A. F.; Brockner, W. *Monatsh. Chem.* **1976**, *107*, 433.
(28) Zinn, A.; Patt-Siebel, U.; Müller, U.; Dehnicke, K. *Z. Anorg. Allg. Chem.* **1990**, *591*, 137.
(29) Faegri, K.; Martinsen, K.-G.; Strand, T. G.; Volden, H. V. *Acta. Chem. Scand.* **1993**, *47*, 547.
(30) Pershina, V.; Sepp. W.-D.; Bastug, T.; Fricke, B.; Ionova, G. V. *J. Chem. Phys.* **1992**, *97*, 1123.
(31) Bauschlicher, C. W. Jr.; Taylor, P. R.; Komornicki, A. *J. Chem. Phys.* **1990**, *92*, 3982.
(32) Tossel, J. A. *Chem. Phys. Lett.* **1990**, *169*, 145.
(33) Tossel, J. A. *J. Phys. Chem.* **1991**, *95*, 366.
(34) Dymek, C. J.; Einarsrud, M.-A.; Wilkes, J. S.; Øye, H. A. *Polyhedron* **1988**, *7*, 1139.
(35) Ystenes, M. *Spectrochim. Acta* **1994**, *50A*, 219.
(36) Einarsrud, M.-A.; Rytter, E.; Ystenes, M. *Vibr. Spectrosc.* **1990**, *1*, 61.

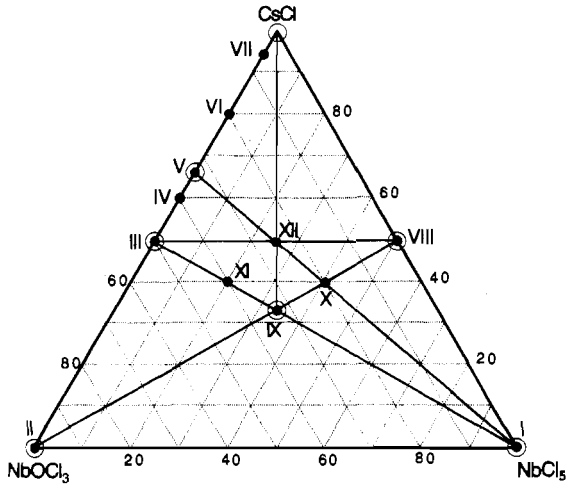

Figure 1. Compositions of the different samples studied plotted in a quasi-ternary diagram $CsCl-NbOCl_3-NbCl_5$. Compositions marked with a circle are reported[6-10] to be stable solid compounds.

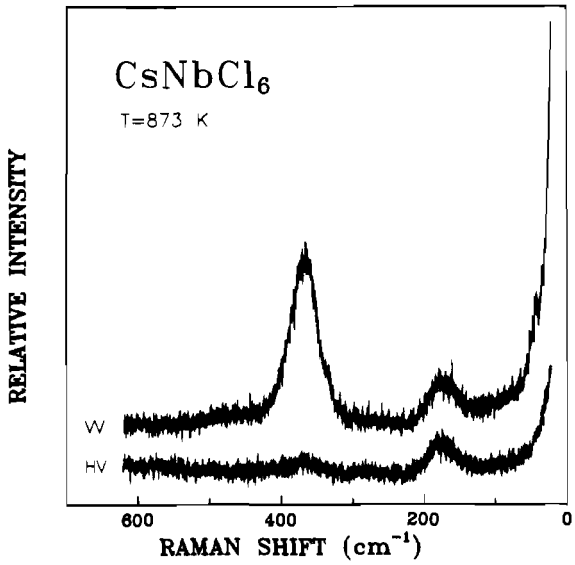

Figure 2. Raman spectra of $CsNbCl_6$ at 500 °C. VV and HV refer to the direction of polarization of the laser light entering and exiting the sample. VV indicates that incident and scattered radiation is polarized perpendicular to the scattering plane. HV indicates that incident radiation is polarized in the scattering plane and the scattered radiation analyzed perpendicular to the scattering plane.

molten mixtures was kept below 20% of the total volume. To record the spectra, the cell was introduced into a specially designed furnace allowing transmission of laser light and collection of scattered light at an angle of 90° to the laser beam.[37] The temperatures were kept just above the melting points of the samples to avoid too high vapor pressures. The compositions of the samples are given in Table 2 and in Figure 1.

The excitation source was a krypton laser emitting red light at 647.1 nm with a power of typically 100 mW. The scattered light was analysed by a Spex 1403, 0.85 m double monochromator, equipped with an RCA photomultiplier cooled to −20 °C and an EG&G/ORTEC photoncounter and a rate meter connected to a PC. Spectra with both horizontal and vertical polarized laser beams were recorded. The slits of the monochromator were adjusted to give a resolution of 3 cm^{-1}. Some of the spectra given show a sharp peak at 97 cm^{-1} which is due to a plasma line at 651.1 nm.

(37) Papatheodorou, G. N. In *Proceedings of the 10th Materials Research Symposium on Characterization of High Temperature Vapors and Gases*; Hastie, J., Ed; NBS Publication 561-1; National Bureau of Standards: Washington, DC, 1979; p 647.

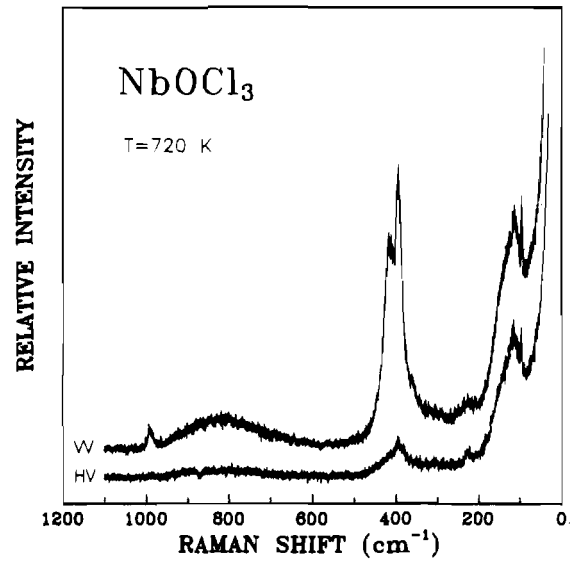

Figure 3. Raman scattering of $NbOCl_3$ at 440 °C.

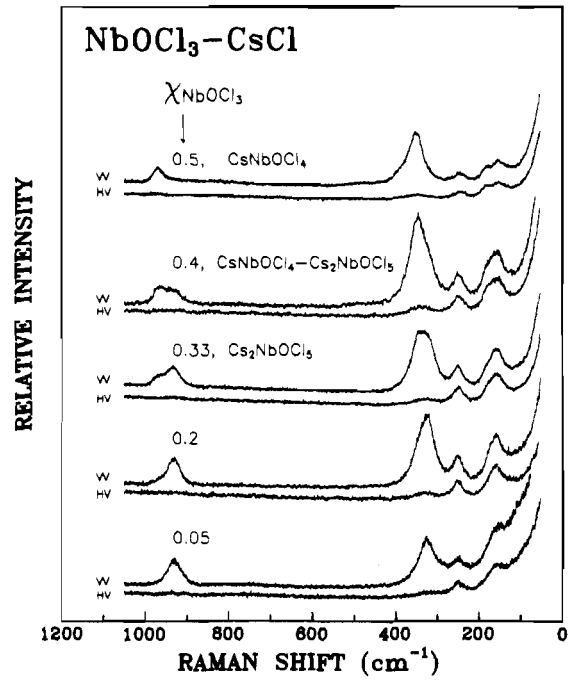

Figure 4. Raman spectra of five melts with different compositions in the system $CsCl-NbOCl_3$. From the bottom and up, the compositions and temperatures in the melts were as follows: 5%$NbOCl_3$ in CsCl at 650 °C; 20%$NbOCl_3$ in CsCl at 630 °C; 33%$NbOCl_3$ in CsCl at 650 °C; 40%$NbOCl_3$ in CsCl at 630 °C; 50%$NbOCl_3$ in CsCl at 560 °C.

Results

General Observations. $NbCl_5$ melts at 205 °C and has a vapor pressure of 1 atm at 250 °C. Both the melt and the gas phase have a deep, orange color. $CsNbCl_6$ melts at 470 °C,[6] and the color of molten $CsNbCl_6$ is deeply red, almost black. An orange color of the vapor phase, indicating a relatively high vapor pressure of $NbCl_5$, was observed above pure melted $CsNbCl_6$. The same orange color was seen also when moving into the $CsCl-NbCl_5-NbOCl_3$ ternary. The pressure of $NbCl_5$ above the melts, indicated by the intensity of color, decreased with increasing n_O/n_{Nb} ratio, and the gas phase above the melts had no color when $n_O/n_{Nb} = 1$.

The amount of CsCl also influenced the pressure of $NbCl_5$. A cell containing the mixture $CsNb_2OCl_9$ exploded at 500 °C due to a vapor pressure estimated to be 10 atm. A 1:1 mixture

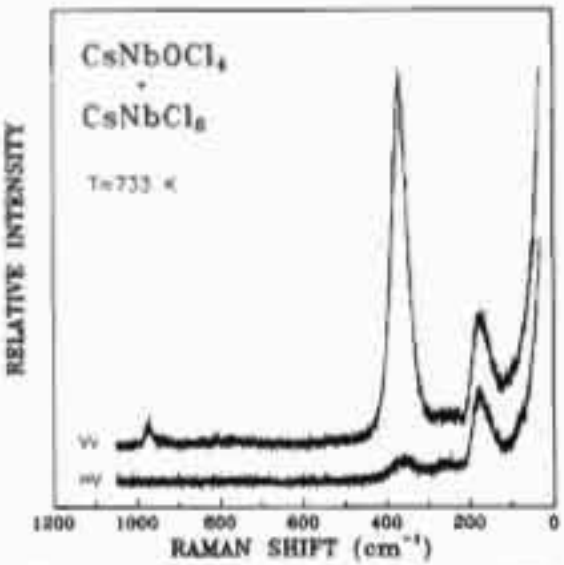

Figure 5. Raman spectra of $CsNbOCl_4$ + $CsNbCl_6$ at 460 °C.

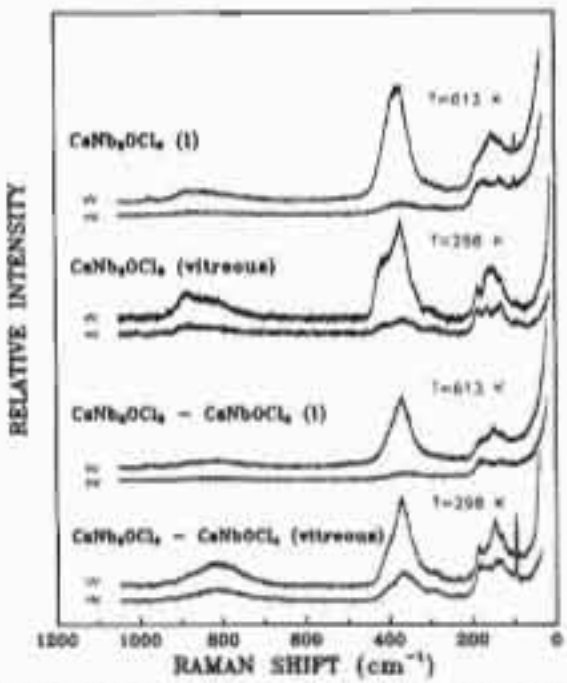

Figure 6. Raman spectra of vitreous and liquid $CsNb_2OCl_6$ + $CsNbOCl_4$ at 340 and 25 °C, respectively (two lower sets), and vitreous and liquid $CsNb_2OCl_6$ at 340 and 25 °C, respectively (two upper sets).

of $CsNbCl_6$ and $CsNbOCl_4$ melted at ~450 °C, and the color of the gas phase above the melt was only weakly yellow, indicating a low $NbCl_5$ pressure. Moreover, as the O/Nb ratio increased, there was a gradual change from the deep red color of $CsNbCl_6$ to the yellow color of molten $CsNbOCl_4$ and Cs_2NbOCl_5.

The dissolution of Nb_2O_5 was much faster in the $CsCl-NbCl_5$ mixtures than in pure $NbCl_5$, probably due to the higher temperature used for the mixture. By mixing $NbCl_5$ and Nb_2O_5 in a 3:1 molar ratio, we obtained needlelike crystals typical of $NbOCl_3$.

Attempts were made to prepare a mixture with $n_O/n_{Nb} > 1$ from a mixture of Nb_2O_5 and $NbCl_5$ in CsCl to produce $NbO_2Cl_x^{(x-1)-}$ complexes. Nb_2O_5 did not dissolve completely even when this mixture was heated above the melting point of CsCl (645 °C) for about 20 min. Spectra of the melt were recorded, and only bands belonging to $NbOCl_5^{2-}$ were observed.

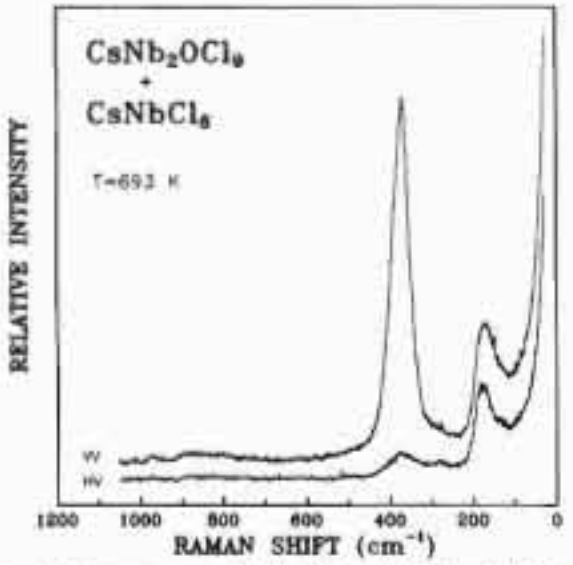

Figure 7. Raman spectra of $CsNb_2OCl_9$ + $CsNbCl_6$ at 420 °C.

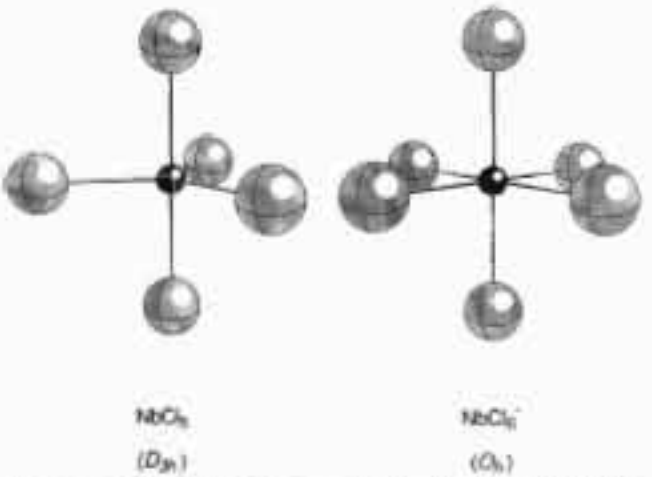

Figure 8. Ball and stick drawings of the calculated geometries (SCF) and $NbCl_5$ and $NbCl_6^-$. Central atoms are niobium, while larger spheres are chlorine.

Experimental Spectra. The spectra of molten $CsNbCl_6$ are shown in Figure 2. Spectra have also been recorded in $CsCl-NbCl_5$ at 500 °C with more than 60% $NbCl_5$. The system has in this composition region two liquids.[8] The lower dark liquid showed peaks belonging to $NbCl_6^-$, and the upper deep orange liquid showed peaks belonging to $NbCl_5$(l).

Since no compounds have been reported in the binary $NbCl_5-NbOCl_3$,[9] no spectra in this concentration region were recorded. However, spectra of molten $NbOCl_3$ have been recorded and are shown in Figure 3. Spectra of several compositions were recorded in the binary $CsCl-NbOCl_3$. The spectra are shown in Figure 4. Figure 5 shows spectra of a mixture of $CsNbCl_6$ and $CsNbOCl_4$ at 460 °C. Figure 6 shows spectra of liquid and vitreous $CsNb_2OCl_6$ at respectively 340 and 25 °C and spectra of liquid and vitreous mixtures of $CsNb_2OCl_6$ and $CsNbOCl_4$ at the same temperatures. Figure 7 shows spectra of a mixture of $CsNb_2OCl_6$ and $CsNbCl_6$. The vibrational bands observed in the spectra are summarized in Table 3.

Quantum Chemical Calculations. The computational details are given in the appendix. For $NbCl_6^-$ we have included results from calculations both with effective core potentials (ECP) and all electron calculations (ECP on niobium), to verify that this simplification does not significantly influence the results. Tables 4 and 5 compare the experimental and theoretical geometries and vibrational frequencies for $NbCl_5$ and $NbCl_6^-$.

Table 3. Wavenumbers and Characteristics of Bands Observed in the Spectra of the Different Samples[a]

	$NbCl_5$	$NbOCl_3$	$CsNbCl_6$	$CsNbOCl_4$	Cs_2NbOCl_5	Cs_2NbOCl_5 + 2CsCl	Cs_2NbOCl_5 + 17 CsCl	Cs_2NbOCl_5 + $CsNbOCl_4$	$CsNb_2OCl_9$	$CsNb_2OCl_9$ + $CsNbCl_6$	$CsNb_2OCl_9$ + $CsNbOCl_4$	$CsNbOCl_4$ + $CsNbCl_6$
temp (°C)	334	440	600	560	650	630	650	630	340	420	340	460
bands		993 w (p)		970 m (p)	970 sh (p)			970 m (p)	970 w (p)	970 w (p)	971 w (p)	971 w (p)
					932 m (p)	932 m (p)	932 m (p)	932 m (p)				
		~825 w, vbr (p)		~825 w, vbr (p)					885 m, br (p)	870 w, br (p)	850 w, br (p)	
									774 vw, br (p)			
									(414 sh (p))			
	414 sh (p)	415 s (p)							391 sh (p)	390 sh (p)		
	393 s (p)	394 s (p)							370 s (p)	369 s (p)	369 s (p)	370 s (p)
			368 s (p)							(349 sh)		(349 sh (p))
				349 s (p)	348 s (p)			348 s (p)				
					323 s (p)	322 s (p)	323 s (p)	323 sh (p)				
	315 m		288 vw						289 sh (p)	281 sh (p)		
				247 m (dp)	249 m	248 m	249 m	246 m				250 vw (dp)
		228 vw									223 vw	
	181 m		176 m (dp)	184 m (dp)	179 sh (dp)	(176 sh)		179 sh	175 sh (dp)	175 m (dp)	175 sh (dp)	178 m (dp)
	150 m	145 sh (p)		155 m (dp)	157 m (dp)	156 m (dp)	155 m	152 m	151 m (p)	151 m (p)	147 m (p)	151 w (dp)
		(123 sh)							129 sh (dp)	129 sh (dp)	129 sh (dp)	
	115 w	114 m (dp)										

[a] Abbreviations: s, strong; m, medium; w, weak; v, very; sh, shoulder; br, broad; p, polarized; dp, depolarized. Wavenumbers are in cm^{-1}. Intensities are visual estimates.

Table 4. Calculated Geometry and Vibrational Frequencies/IR Intensities for Molecular $NbCl_5$, Compared with Experimental Vibrational Frequencies[a]

assignments	obsd[b]	SCF[c]	PED[d]	VFF[e]
r_1 (Nb−Cl_{eq})		2.285		
r_2 (Nb−Cl_{ax})		2.345		
E′	54	55/0.08	r_1; 41; α, 91; β, 163	100
E′	148	151/0.2	α, 16, β, 94	156
A_2''	184	186/0.3	β, 75	126
E″	180	199	β, 68	145
A_1'	317	305	r_1, 44; r_2, 75	314
A_2''	396	381/7	r_2, 125; β, 4	394
A_1'	394	401	r_1, 53; r_2, 20	358
E′	430	430/3	r_1, 105	440

[a] Bond lengths in Å, angles in deg, vibrational frequencies (wavenumbers) in cm^{-1}, intensities in $D^2\ u^{-1}\ Å^{-2}$, bondlengths in Å, PED in % in this and the following tables. [b] From refs 11 and 19, except for the A_2'' modes taken from refs 38 and 39. [c] The diagonal and main off-diagonal valence force constants are (F and f in mdyn/Å, H in mdynÅ/rad²): F_{r_1}, 2.600 (2.61); F_{r_2}, 2.135 (1.94); H_α, 0.181 (0.59); H_β, 0.812 (0.57); $f_{r_1r_1}$, 0.135; $f_{r_2r_2}$, 0.237; $f_{r_1r_2}$, 0.267. (Numbers in parentheses behind the force constants are values found by Nour[40] by a valence force field analysis). [d] On the basis of valence coordinates, contributions below 10% omitted. Key α, Cl_{eq}−Nb−Cl_{eq} angles; β, Cl_{eq}−Nb−Cl_{ax} angles. [e] Valence force field calculations by Nour.[40]

Table 5. Calculated Geometry and Vibrational Frequencies/IR Intensities for $NbCl_6^-$, Compared with Experimental Data

assignments	obsd[a]	SCF (ECP)[b]	SCF[b,c]	PED[c]
r (Nb−Cl)	2.34	2.390	2.395	
T_{2u}		79/0	80/0	α, 110
T_{1u}	162	163/0.5	162/0.5	α, 87
T_{2g}	170−181	179/0	178/0	α, 58
E_g	288−281	272/0	271/0	r, 112
T_{1u}	333	336/7	329/7	r, 90
A_{1g}	366−373	366/0	364/0	r, 63

[a] Experimental bond length (Å) from ref 41; experimental frequencies (cm^{-1}) from refs 11 and 12. [b] The first data set is obtained with effective core potentials on chlorine, whereas the second set is obtained with an all electron description of chlorine (cf. Appendix). [c] The diagonal and the most important off-diagonal force constants are (F and f in mdyn/Å, H and h in mdynÅ/rad²) as follows: F_r, 1.715; H_α, 0.542; f_{rr}, 0.20−0.22; $h_{\alpha\alpha}$(no common bond), −0.24. [c] On the basis of the valence force constants, contributions below 10% were omitted.

Table 6. Calculated Geometry and Vibrational Frequencies/IR Intensities for $NbOCl_3$, Compared with Experimental Vibrational Frequencies

assignments	obsd[a]	SCF	CASSCF	scaled[b]	PED[c]
r_1 (Nb−O)		1.642	1.679		
r_2 (Nb−Cl)		2.312	2.324		
α (O−Nb−Cl)		107.9	106.0		
β (Cl−Nb−Cl)		111.0	112.7		
E	106	107	102/0.1	102	β, 93
A_1	133	137	134/0.2	134	α, 22; β, 54
E	225	239	230/0.03	230	β, 70
A_1	395	392	383/0.5	383	r_2, 88
E	448	440	430/3	430	r_2, 97
A_1	997	1164	1049/2	995	r_1, 100

[a] Experimental frequencies ref from 13, except for $\nu_3(A_1)$ taken from ref 38. [b] CASCF values, scale factor for F_{r_1} is 0.9, all others are 1.0. After scaling, the diagonal force constants are (F in mdyn/Å, H in mdynÅ/rad²) as follows: F_{r_1}, 7.92; F_{r_2}; 2.48; H_α, 0.62; H_β, 0.33. [c] Based on the scaled CASSCF valence force field, contributions below 10% omitted.

Ball and stick drawings of the SCF optimized geometries are shown in Figure 8. In Tables 6−8 the calculated data for $NbOCl_3$, $NbOCl_4^-$, and $NbOCl_5^{2-}$ are compared with experimental data, and ball and stick drawings of the complete active

Table 7. Calculated Geometry and Vibrational Frequencies/IR Intensities for $NbOCl_4^-$ Compared with Experimental Geometries and Vibrational Frequencies

assignments	obsd[a]	SCF	CASSCF	scaled[b]	PED[c]
r_1 (Nb−O)	1.74, 1.69, 1.67	1.648	1.682		
r_2 (Nb−Cl)	2.38, 2.40, 2.38	2.435	2.446		
α (O−Nb−Cl)	98.3, 97.7, 97.8	104.0	102.6		
β (Cl−Nb−Cl)	88.8, 88.9, 89.0	86.7	87.3		
B		46	47/0	47	r_3, 10; β, 260
E		147	141/0.2	141	α, 84
A_1	150	161	157/0.3	156	r_3, 2, α, 10; β, 44
B_2	165	186	179/0	179	α, 75
E	232 237	251	238/0.003	238	β, 86; r_3, 12
B_2	268	259	258/0	258	r_2, 116
A_1	312−333	342	333/0.4	333	r_2, 73
E	313−315	358	347/5	347	r_3, 104; β, 13
A_1	942−962	1146	1044/2	935	r_1, 99

[a] Experimental geometries and frequencies from refs 20, 42, and 43. [b] Scale factor for $F_{r_1} = 0.8$, all others were 1.0. After scaling, the diagonal force constants are (F in mdyn/Å, H in mdynÅ/rad²) as follows: F_{r_1}, 6.96; F_{r_2}, 1.59; H_α, 0.65, H_β, 0.78. [c] On the basis of the scaled CASSCF valence force field, contributions below 10% were omitted.

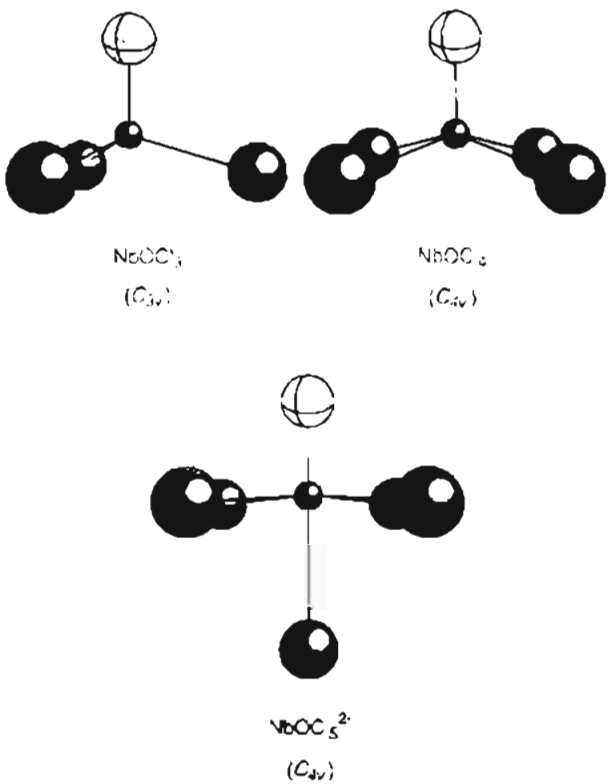

Figure 9. Ball and stick drawings of the CASSCF optimized geometries of $NbOCl_3$, $NbOCl_4^-$, and $NbOCl_5^{2-}$. Central atoms are niobium. Oxygen atoms are given as smaller and lighter spheres than chlorine.

space SCF (CASSCF) optimized geometries are shown in Figure 9. For comparison calculations were performed for the homologous species $VOCl_3$ and $VOCl_4^-$ and experimental data and theoretical results are given in Tables 9 and 10. Ball and stick models of $VOCl_3$ and $VOCl_4^-$ drawn according to the SCF-optimized geometries are shown in Figure 10. Finally we have calculated the energy change for the reaction $NbOCl_4^- + Cl^- = NbOCl_5^{2-}$. As seen in Table 11 the calculation performed on free ions is not convincing. Using overall neutral model compounds (see Figure 11), much more reasonable data are obtained, especially for the MP2 energy calculations (CASSCF geometry). The MP2 method is the most reliable for energy calculations since SCF and CASSCF calculations will underestimate the increase in correlation energy on the formation of a new bond.

Discussion

Sample Preparation. The Gibb's free energy for the reactions

$$3NbCl_5(g) + Nb_2O_5(s) = 5NbOCl_3(g) \quad (1)$$

and

$$2NbCl_5(g) + SiO_2(s) = 2NbOCl_3(g) + SiCl_4(g) \quad (2)$$

are respectively −133.2 and −21.6 kJ mol^{-1}[49] indicating that both Nb_2O_5 and fused silica can dissolve in melts containing $NbCl_5$. However, Raman spectra of Nb(V)−chloride melts without oxide additions kept in fused silica cells at 550 °C for an hour showed no oxide bands. However, when oxide free melts were exposed to fused silica at temperatures above 650 °C, oxide bands appeared in the spectra after about an hour. After several hours, only bands belonging to niobium oxochloride species could be observed. When $NbOCl_3$ was prepared from stoichiometric amounts of Nb_2O_5 and $NbCl_5$, not all of the Nb_2O_5 dissolved and some $NbCl_5$ was present in the gas phase. However, the amount of undissolved Nb_2O_5 was small, and the volume of the gas phase was lower than that of the melt. Moreover, monomeric $NbCl_5$ should give a medium strong band at 316 cm^{-1}, but this is not present in the spectrum of molten $NbOCl_3$ (Figure 3). It is therefore reasonable to assume that unreacted Nb_2O_5 and $NbCl_5$ were present in the cell as solid Nb_2O_5 and gaseous $NbCl_5$, and that the melt mainly was $NbOCl_3$. The spectra of this melt is therefore probably representative of liquid $NbOCl_3$.

(38) Zavalishin, N. I.; Mat'izev, A. A. *Vestn. Mosk. Univ.* **1976**, *3*, 314.
(39) Werder, R. D.; Fray, R. A.; Gunthard, H. S. *J. Chem. Phys.* **1967**, *47*, 4159.
(40) Nour, E. M. *Spectrochim. Acta* **1986**, *42A*, 1411.
(41) Gaebell, H. C.; Meyer, G.; Hoppe, R. *Z. Anorg. Allg. Chem.* **1982**, *493*, 65.
(42) Klingelhöfer, P.; Müller, U. *Z. Anorg. Allg. Chem.* **1984**, *516*, 85.
(43) Aspinall, H. C.; Roberts, M. M. *Inorg. Chem.* **1984**, *23*, 1782.
(44) Palmer, K. J. *J. Am. Chem. Soc.* **1938**, *60*, 2360.
(45) Brockner, W.; Jendrzok, B.; Menzel, F.; Jensen, V. R.; Ystenes, M. *J. Mol. Struct.* **1994**, *319*, 85.
(46) Willing, W.; Christophersen, R.; Müller, U.; Dehnicke, K. *Z. Z. Anorg. Allg. Chem.* **1987**, *555*, 16.
(47) Chritchlow, S. C.; Lerchen, M. E.; Smith, R. C.; Doherty, N. M. *J. Am. Chem. Soc.* **1988**, *110*, 16.
(48) Øye, H. A.; Jagtøyen, M.; Oksefjell, T.; Wilkes, J. S. *Proceedings from the Ketil Motzfeldt Symposium*, NTH: Trondheim, Norway, 1991; p 33.
(49) Barin, I. *Thermochemical data of Pure Substances*, VCH: Mannheim, Germany, 1989.

Table 8. Calculated Geometry and Vibrational Frequencies/IR Intensities for $NbOCl_5^{2-}$ Compared with Experimental Data

assignments	expt[a]	SCF	CASSCF	scaled[b]	PED[c]
r_1 (Nb−O)	*d*	1.664	1.709		
r_2 ($Nb-Cl_{eq}$)	2.41	2.505	2.524		
r_3 ($Nb-Cl_{ax}$)	2.555	2.703	2.661		
α ($O-Nb-Cl_{eq}$)	93.7	93.2	91.8		
β ($Cl_{eq}-Nb-Cl_{eq}$)	89.8	89.8	88.2		
γ ($Cl_{eq}-Nb-Cl_{ax}$)	86.5	86.8	89.9		
E	85−87	83	83/0.0004	90	β, 67; γ, 52; α, 16
B_1	97	98	98/0	107	α, 42; β, 39
E	156	145	141/0.01	155	γ, 38, β, 42
B_2	167?	149	145/0	159	β, 69
A	179?	165	163/0.05	179	γ, 24; α, 23
A_1	231−234	196	213/1.4	233	r_3, 93, r_2, 20
B	248	231	228/0	251	r_2, 104
E	?	266	247/0.4	271	α, 74
E	≈300	285	279/5.5	306	r_2, 125
A_1	324−330	298	292/0.5	320	r_3, 53; r_1, 18
A_1	928−932	1102	972/3.1	922	r_1, 100

[a] Experimental geometry from ref 21 and frequencies from the present work and refs 14 and 15. [b] Scale factor for F_1 = 0.9, all others were 1.2. After scaling, the diagonal force constants are (*F* in mdyn/Å, *H* in mdynÅ/rad²) as follows: F_{r_1}, 6.83; F_{r_2}, 1.38; F_{r_3}, 0.97; H_α, 0.63; H_β, 0.58; H_γ, 0.60. [c] On the basis of the scaled CASSCF valence force field, contributions below 10% were omitted. [d] The paper[21] gives the distance as 1.967 Å, but this result is highly questionable. See text.

Table 9. Calculated Geometry and Vibrational Frequencies/IR Intensities for $VOCl_3$ Compared with Experimental Vibrational Frequencies

assignments	obsd[a]	SCF	scaled[b]	PED[c]
r_1 (V−O)	1.56	1.497		
r_2 (V−Cl)	2.12	2.146		
α (O−V−Cl)	108.2	108.4		
β (Cl−V−Cl)	111.3	110.6		
E	125−132	134/0.02	128	α, 90
A_2	163−173	180/0.06	170	β, 28; α, 48
E	248−250	284/0	269	r_2, 21; α, 72
A_1	408−411	437/0.5	415	r_2, 75
E	502−507	534/5	507	r_2, 93
A_1	1035−1043	1295/7	1047	r_1, 99

[a] Experimental frequencies from refs 13, 26, 17, and 38. Note that the two lowest frequency bands were reversed by ref 13 based on polarization measurements, but both the polarization measurement and the assignment have been corrected by ref 38. Experimental gas phase electron diffraction data for $VOCl_3$ were from ref 44. [b] Scaling factors: 0.65 for F_α, 0.9 for the other. After scaling, the diagonal force constants were (*F* in mdyn/Å, *H* in mdynÅ/rad²) as follows: F_{r_1}, 7.79; F_{r_2}, 2.64; H_α, 0.64; H_β, 0.42. [c] On the basis of the scaled force field and valence force constants, contributions below 10% were omitted.

The Binary CsCl−$NbCl_5$. The spectra of pure $NbCl_5$ and $CsNbCl_6$ (Figure 2) showed no peaks in the region of the oxide bands, indicating a negligible corrosion of the fused silica cell used. No visual signs of corrosion of the cell could be observed after the measurement.

The Binary $NbCl_5$−$NbOCl_3$. Most of the features of the gaseous spectrum of $NbOCl_3$ are present in the spectra in Figure 3, such as the polarized band of the terminal Nb=O stretch at 993 cm^{-1}, the polarized Nb−Cl stretching band at 394 cm^{-1}, and the bands at 228 and 114 cm^{-1} (cf. Table 6). Monomeric $NbOCl_3$ is therefore probably present in the melt. In addition there is a polarized band at 420 cm^{-1}, similar to what is found in $NbOCl_3$(s), and a broad polarized band at ~800 cm^{-1}, which is probably due to bridging oxygen. The band assigned to the bridging oxygen in the solid is reported to be very sharp,[13] while the corresponding band in the melt is very broad. This may hint to a broad range of configurations of ions with bridging oxygen in the melt, or to a very short lifetime of the bridge. Polymeric $NbOCl_3$ similar to that found in the solid may therefore be present in the melt.

Table 10. Calculated Geometry and Vibrational Frequencies/IR Intensities for $VOCl_4^-$ Compared with Experimental Vibrational Frequencies and Geometries

assignments	obsd[a]	reassigned[b]	SCF	scaled[c]	PED[d]
r_1 (V−O)	1.55−1.61		1.498		
r_2 (V−Cl)	2.23−2.26		2.291		
α (O−V−Cl)	101−103		103.6		
β (Cl−V−Cl)	88		86.8		
B_1			49	49	r_2:20, β:300
E	165 s	165 s (?)	184/0.1	184	α:83
A			207/0.06	207	α:12; β:40
B_2	252 m		225/0.06	225	α:75
B	363 mb	252 m	259	259	r_2:126
E			290/0.3	290	β:69; r_2:25
A_1	403 m	363 mb	369/0.3	369	r_1:68
E	420 m	420 m (403)	428/6	428	r_2:95; β:27
A	1023 s	1023 s	1283/6	1040	r_1:97

[a] Geometry from refs 28, 46, and 47, vibrational frequencies from ref 28; m = medium, s = strong, and b = broad. [b] The broad A mode and splitting of the E-mode is taken as evidence of distortion of the ion leading to reduced symmetry. The 165 cm^{-1} band may be strongly influenced by or due to lattice vibrations. [c] F_α scaled 0.70, the others 1.0. After scaling, the diagonal force constants were (*F* in mdyn/Å, *H* in mdynÅ/rad²) as follows: F_{r_1}, 7.54; F_{r_2}, 1.75; H_α, 0.77; H_β, 1.09. [d] On the basis of the scaled SCF field, contributions below 10% were omitted.

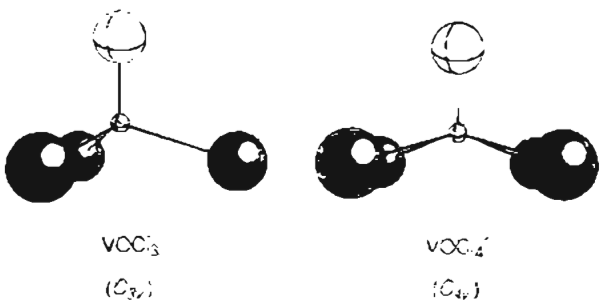

Figure 10. Ball and stick models of $VOCl_3$ and $VOCl_4^-$ drawn according to the calculated geometries (SCF). Central atoms are vanadium. Oxygen atoms are given as smaller and lighter spheres than chlorine.

The Binary CsCl−$NbOCl_3$. Melts dilute in $NbOCl_3$ show strong polarized bands at 324 and 923 cm^{-1}, typical of the $NbOCl_5^{2-}$ ion (cf. Table 8). When the concentration of $NbOCl_3$ is increasing, additional bands show up at 348 and 970 cm^{-1}.

Table 11. Calculated Energy Change (kJ/mol) for the reaction $NbOCl_4^- + Cl^- = NbOCl_5^{2-}$

reaction	method	$\Delta E°$
$NbOCl_4^- + Cl^- = NbOCl_5^{2-}$	SCF	156
$NaNbOCl_4 + NaCl = Na_2NbOCl_5$[a]	SCF	−70
	CASSCF	−93
	MP2	114

[a] The geometries are shown in Figure 5. The Na$^+$'s were confined to be in-plane with Nb and the two bridging Cl's to ensure equal Na Cl bonding conditions for the two model species.

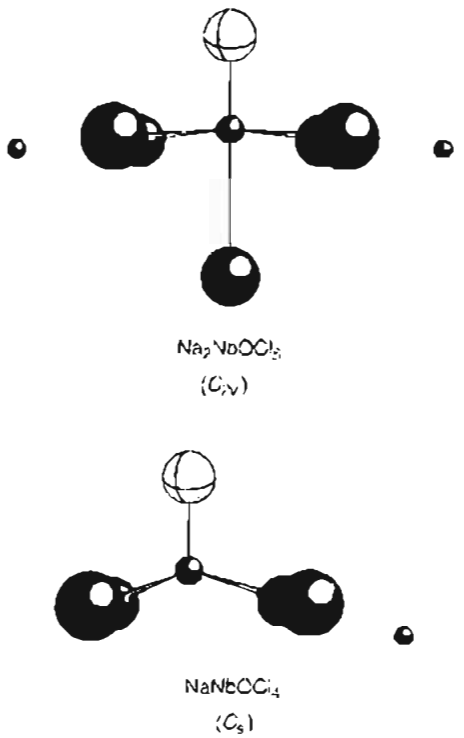

Figure 11. Ball and stick drawings of the CASSCF optimized geometries of the model compounds $NaNbOCl_4$ and Na_2NbOCl_5 used to estimate the equilibrium constant of the reaction $NbOCl_4^- + Cl^- = NbOCl_5^{2-}$. (See Table 11.) The Na atoms were forced to be in-plane with Nb and the two bridging Cl atoms; hence, the geometries do not give global energy minima. Central atoms are niobium. Oxygen atoms are given as smaller and lighter spheres than chlorine, and small and dark atoms not connected with sticks are Na atoms.

At the composition $CsNbOCl_4$, the bands belonging to $NbOCl_5^{2-}$ disappear, and it is reasonable to conclude that the spectrum at this composition shows bands of the $NbOCl_4^-$ ion, including a symmetrical Nb−Cl stretch at 348 cm^{-1} and a symmetrical Nb=O stretch at 970 cm^{-1} (cf. Table 7). Thus, in the binary CsCl−$NbOCl_3$ at $x_{NbOCl_3} < 0.5$, the equilibrium

$$Cs_2NbOCl_5 = CsCl + CsNbOCl_4 \qquad (3)$$

seems to be established. Assuming that equal concentrations of $NbOCl_4^-$ and $NbOCl_5^{2-}$ lead to peaks of similar intensities, the equilibrium constant (pure component standard state) of reaction 3 is close to unity. However, since these binary melts were slightly colored, preresonance between the exciting laser and charge transfer bands may occur, and the estimated concentrations of $NbOCl_4^-$ and $NbOCl_5^{2-}$ based on the spectra may be misleading. Quantum chemical calculations (cf. Table 11) of the energy change for a similar reaction $NaNbOCl_4 + NaCl = Na_2NbOCl_5$, gave a negative energy change. This will drive the reaction to the right, but the higher entropy on the left side of the reaction will oppose this driving force, leading to a Gibbs free energy change considerably less negative than the calculated $\Delta E°$. The quantum chemical calculations therefore support the observed equilibrium for reaction 3. However, neither the Raman spectra nor the calculations allow an accurate determination of the equilibrium constant for reaction 3.

In a mixture of 5% $NbOCl_3$ and 95% CsCl, only bands belonging to $NbOCl_5^{2-}$ were observed. Bands due to a possible $NbOCl_6^{3-}$ ion could not be detected.

The Ternary CsCl−$NbCl_5$−$NbOCl_3$. Spectra recorded of melts with compositions within this ternary system strongly reflect its acid−base properties. As Cl$^-$ ions are removed, i.e., the CsCl concentration is reduced, the melt becomes more acidic. To compensate for the loss of Cl$^-$ ions, the negative Nb containing ions tend to share the remaining chloride and oxide ions by forming bridging bonds. Figure 5 shows spectra of a 1:1 mixture of $CsNbOCl_4$ and $CsNbCl_6$. Peaks typical of the $NbOCl_4^-$ and $NbCl_6^-$ ions are the major features of these spectra. These species are believed to be the main complex ions in such melts.

When the CsCl concentration is reduced to 33.3% and $x_{NbCl_5} = x_{NbOCl_3} = 33.3\%$, the melt becomes more acidic. This melt can be considered as 1:1 mixtures of $CsNbCl_6$–$NbOCl_3$ or $CsNbOCl_4$–$NbCl_5$ or simply as molten $CsNb_2OCl_9$. It is interesting to notice that this mixture formed a glass when the cell was cooled quickly in air or water. Both spectra of the glass and the liquid (Figure 6) show the strong polarized bands of the symmetrical Nb−Cl stretching between 370 and 410 cm^{-1}. Probably several Nb−O−Cl and Nb−Cl complexes coexist both in the melt and in the glass.

It is difficult to decide which complexes are present, but some suggestions can be made. In the spectrum of the liquid a small peak can be seen at 970 cm^{-1}. This is the same position as the peak of the terminal Nb=O stretch in $NbOCl_4^-$ (cf. Table 7). This peak is not visible in the spectrum of the glass. There are also several bands between 780 and 890 cm^{-1}, suggesting that both the melt and the glass contain bridging oxygen. The relatively high values of the wavenumbers (between 370 and 410 cm^{-1}) of the polarized Nb−Cl stretching bands indicate fairly strong Nb−Cl bonds. These values are comparable to the wavenumbers of Nb−Cl stretching bands in spectra of molten $NbOCl_3$ (394 and 415 cm^{-1}), Nb_2Cl_{10} (415 cm^{-1}), $NbCl_5$ (397 cm^{-1}) and $NbCl_6^-$ (368 cm^{-1}) (cf. Tables 4−6). From these observations it is reasonable to assume that both monomeric species with terminal oxygen and polymeric species with bridging oxygen are present in the melt, while the glass contains mostly polymeric species with bridging oxygen. Moreover, the presence of terminal oxygen in the melt implies that complexes without oxides also exist since the niobium to oxide ratio, $n_{Nb}/n_O = 2$. Since the melt forms a glass when it is cooled fairly rapidly, the melt is probably partly polymerized.

Not only the acidity of the melt is important, also the oxygen concentration seems to be essential for the formation of polymers. The spectra of melts with the 1:1 compositions $CsNbCl_6$–$CsNb_2OCl_9$ (Figure 7) and $CsNbOCl_4$–$CsNb_2OCl_9$ (Figure 6) illustrate this point. The latter melt was also glass forming when the cell was cooled in water. The spectra are very similar to the spectra of the $CsNb_2OCl_9$ mixture, and thus the complexes in this melt are probably mainly the same as in the $CsNb_2OCl_9$ melt. It is noteworthy that the spectra of the glass do not show any sign of the terminal oxide band at 970 cm^{-1}, only the band of the bridging oxygen at around 850 cm^{-1}. This indicates that terminal oxygen atoms in the $NbOCl_4^-$ ions become bridged to other Nb atoms when the glass is formed even when $n_O/n_{Nb} > 0.5$, suggesting polymers with several bridging oxygen atoms and accordingly more than two Nb atoms per polymer.

The 1:1 $CsNbCl_6$–$CsNb_2OCl_9$ did not form a glass. Bands typical for $NbCl_6^-$ are the major features in these spectra (Figure 7). The broad peak at ~850 cm^{-1} indicates some bridging oxygen, while the peak at 970 cm^{-1} and the weak shoulder at 348 cm^{-1} show that $NbOCl_4^-$ is also present. In addition there is a weak shoulder at ~390 cm^{-1}, probably having the same origin as the peaks in the $CsNb_2OCl_9$ mixture. The degree of polymerization, however, seems to be smaller in the $CsNbCl_6$–$CsNb_2OCl_9$ melt than in the $CsNbOCl_4$–$CsNb_2OCl_9$ melt.

Comments to the Quantum Chemical Calculations. For $NbCl_6^-$ the fit between the experimental and calculated frequencies (Table 5) are convincing, the slight overestimation of the bond length is quite normal for charged species (see, e.g., ref 50). For $NbCl_5$ (Table 4), for which no direct geometry determination is known, the fit is less convincing. It should, however, be noted that there is a considerable disagreement between the reported vibrational spectra.[11,19,38,41] Some erroneous assignments given earlier, including one based on a normal coordinate analysis[40] (see Table 4), may also have led to confusion.

For $NbOCl_3$ (Table 6) no experimental geometries are reported, and for $NbOCl_4^-$ (Table 7) such data are known only where organic ligands are associated with the central Nb atom, almost making it six-coordinate.[20,42,43] However, comparing the experimental frequencies with the observed spectra reveal a very strong calculated Nb–O bond for $NbOCl_3$, $NbOCl_4^-$, and $NbOCl_5^{2-}$ at the SCF level. CASSCF calculations improve the fit significantly and show that this problem is due to near-degeneracy. Still a scaling down of the Nb–O stretching force constant is needed to obtain a satisfactory fit. The need for scaling indicate that even more states should be included in the CASSCF calculations. With this scaling, most modes are modelled within a deviation of 5%, and large deviations are not observed.

The deviations are in general smaller than those seen for the geometry of $MoCl_5$ calculated at a similar level.[29] Hence it seems safe to conclude that the calculations give a good picture of the given species, and the absence of imaginary modes verify their symmetries. In contrast, the deviation between the calculated and experimental bond distance[21] for Nb=O in $NbOCl_5^{2-}$ (Table 8) is dramatic and must be due to a significant error in either the theoretical or the experimental work. Despite the influence of the charge (see below), we feel, for several reasons, that it is reasonable to rely on the calculations. (1) The experimental bond length is very much longer than what is found for all the other Nb–O–Cl species, and indicates a single bond, or even less. This is not reflected in the Nb–O stretching frequency, which is only slightly lower than that for $NbOCl_4^-$. (2) The difference between the scaling factors for Nb–O and Nb–Cl stretch is not substantially different for the three species. (3) There are some peculiarities in the crystallographic study, such as an isotropic refinement for oxygen whereas all other atoms are refined anisotropically, and the temperature factor for Nb toward O is very large. (4) The experimental study shows a longer axial Nb–Cl bond, which does not make sense unless the Nb–O bond is stronger than a normal single bond.

For charged species calculated as free ions there will in general be an overestimation of bond lengths, due to a too high electrostatic repulsion between the atoms within the ion. In a real ionic lattice this repulsion will be reduced due to the polarizability of the cations, i.e., the charge of the ions is in general significantly lower than the perfect integral charge assumed. If the ligands of the anion have different polarizability, this elongation effect will show up mainly for the most polarizable ligands (compare e.g. the 15% overestimation of the P–S bond relative to the P–O bonds in PSO_3^{3-} [45]). In $NbOCl_5^{2-}$ we see a significant overestimation of the Nb–Cl bond lengths, and the too long $Nb-Cl_{eq}$ bond will in turn tend to shorten the Nb–O bond. As a consequence, the difference in the scaling factors for F_{r_1} and the other parameters is somewhat larger for $NbOCl_5^{2-}$ than for the other Nb–O–Cl species.

In the model compound Na_2NbOCl_5 (see Figure 11) the calculated (SCF) Nb–O and $Nb-Cl_{ax}$ bond lengths are 0.02 and 0.12 Å shorter, respectively, compared with the free anion. The $Nb-Cl_{eq}$ bonds have almost exactly the same length in the two models, although they are not directly comparable. Nevertheless, the calculated geometry of Na_2NbOCl_5 verifies that the charge effect cannot explain the difference between the calculated and experimental Nb–O bond lengths.

Of the vanadium oxochloride compounds, $VOCl_4^-$ (Table 10) is especially interesting since a series of experimental geometries are known. These show clearly the underestimation of the V–O bond length in the SCF calculations. The same deviation is seen for $VOCl_3$, although the rather old electron diffraction data[44] may be uncertain. CASSCF calculations appeared to correct this deviation in the same way as for the Nb homologues, but due to some instabilities in the CASSCF wave functions we have not included the results from the CASSCF calculation. Although the data for the experimental frequencies of $VOCl_4^-$ are incomplete, the fit to the experimental frequencies for the vanadium oxochlorides is convincing after downscaling of the V–O stretching force constants.

Conclusions

Spectra of molten $NbOCl_3$ have been recorded, and evidence for both terminal and bridging oxygen has been found.

When the CsCl content in the melt was higher than 50 mol % and no oxide was present, $NbCl_6^-$ was the major Nb containing complex. When oxide was added to the melt, the oxochlorides $NbOCl_4^-$ and $NbOCl_5^{2-}$ seem to participate in the equilibrium

$$CsNbOCl_4 + CsCl = Cs_2NbOCl_5$$

Quantum chemical calculations on neutral model molecules support the presence of this equilibrium.

In the acidic central regions of the $CsCl$–$NbCl_5$–$NbOCl_3$ system, polymeric ions containing bridging oxygen probably exist. However, complexes with terminal oxygen are also present in these melts, which also were glass forming when cooled rapidly.

Experimental and calculated frequencies and symmetries of ions and molecules occurring in the binary $CsCl$–$NbOCl_3$ are consistent, and we may conclude that (1) the calculated symmetries of the molecules and ions are probably correct, (2) the calculated molecular and ionic geometries seem to be reasonable, and (3) the scaled quantum mechanical calculations seem to give a reliable basis for assignment of the vibrational spectra.

The results also show that quantum chemical calculations of niobium and vanadium species may yield good estimates of geometry, energy, and vibrational frequencies. Significant effects of near-degeneracy may appear that causes the need for CASSCF or similar methods. However, these effects on the vibrational frequencies of the niobium oxochloride species studied may be corrected by simple scaling.

(50) Ystenes, M.; Brockner, W.; Menzel, F. *Vibr. Spectrosc.* **1992**, *3*, 285.

Acknowledgment. This project has benefited scientifically from our participation in a Human Capital and Mobility Network. We appreciate interesting discussions with Prof. W. Freyland, University of Karlsruhe, Germany, and in particular with Prof. G. N. Papatheodorou, University of Patras, Greece, on the structure of niobium chloride containing melts. Financial support from the Research Council of Norway is also gratefully acknowledged. Moreover, a grant of computing time from the Norwegian Supercomputing Committee (TRU) is gratefully acknowledged. The authors also want to thank Intel Corp. for support through the SINTEF/Intel Paragon Supercomputer Partnership Agreement.

Appendix

Computational Details. All geometries and Hessians have been determined at the *ab initio* self consistent field (SCF) level of theory. For species including oxygen, calculations at the complete active space SCF (CASSCF)[51] level of theory have also been performed. The CASSCF calculations were done in order to correlate the two doubly occupied MO's resulting from the oxygen π-like bonding toward the metal with their respective antibonding orbitals, resulting in a multiconfigurational (MC) description including 20 configuration state functions (CSF's). Several (up to six) of these CSF's had coefficients between 0.10 and 0.15, and thus a MC description of the wave function was found to be necessary. Analytic gradients have been used in all cases. The Hessians were obtained from finite differences of the analytically determined gradients, and the corresponding frequencies were calculated using the harmonic approximation.

Because of the size of the systems studied, it has been imperative to include extensive use of effective core potentials (ECP's). For niobium, the relativistic ECP according to Hay and Wadt[52] was used. The 4s and 4p orbitals were described by a single-ζ contraction, the valence 5s and 5p by a double-ζ contraction and the 4d orbitals by a triple-ζ contraction, including one diffuse function. Vanadium was described by Wachters primitive (14s, 9p, 5d) basis set[53] contracted to [10s, 8p, 3d] with some modifications. The most diffuse s function was removed and replaced by one s function spanning the 3s–4s region (α_s = 0.231). Two p functions to describe the 4p region were added (α_p = 0.175, 0.068), and one diffuse d-primitive was added (α_d = 0.1007). For chlorine, the ECP according to Hay and Wadt[54] was used. The valence basis set was double-ζ in the 3s and 3p regions and single–ζ in the 3d region (α_d = 0.75). A SCF calculation on $NbCl_6^-$ with all-electron description of chlorine was also performed as a test (Table 4). In this calculation, chlorine was described by the Dunning and Hay[55] valence double-ζ augmented by one d function with exponent 0.75. Oxygen was described by the Dunning and Hay[55] valence double-ζ basis augmented by one d function with exponent 0.80. For sodium, the ECP according to Hay and Wadt[54] was used and the valence basis set was double-ζ in the 3s and 3p regions. These basis sets and ECP's were used in all geometry optimizations and Hessian calculations reported in this paper.

For the reaction $NaNbOCl_4 + NaCl = Na_2NbOCl_5$, the geometries of the Nb complexes were determined at the SCF and CASSCF levels of theory, with the Na^+ ions constrained to be in the $NbCl_2$-plane, as can be seen in Figure 11. This constraint was necessary in order to obtain an equal treatment of the two Nb complexes, and this also gives the smallest possible difference in geometry compared to the corresponding anions. The NaCl structure was only determined at the SCF level, as no Na or Cl orbitals are included in our active space in the Nb complexes. For these neutral species, second order Møller-Plesset (MP2)[56] energy corrections have been calculated at the stationary points determined at the CASSCF level of theory (SCF level for NaCl). Somewhat larger basis sets were used in the MP2 single point energy evaluations. For niobium, three f primitives contracted to one function were added. The chlorine and oxygen basis sets were augmented by one diffuse p function with exponents 0.052 and 0.064, respectively. For sodium, the basis set was augmented by a d function with exponent 0.175.

All *ab initio* calculations presented in this paper were performed with the electronic structure codes GAMESS[57] and Gaussian.[58] Scaling of force constants, verification of the symmetries of vibrations, and calculations of potential energy distributions were done with the help of the programs GAMFORCE[59] and MOLVIB.[60]

IC941005Y

(51) Roos, B. O. In *Methods in Computational Molecular Physics*; Diercksen, G. H. F., Wilson, S., Eds.; D. Reidel Publishing: Dordrecht, The Netherlands, 1983; pp 161–187.
(52) Hay, P. J.; Wadt, W. R. *J. Chem. Phys.* **1985**, *82*, 299.
(53) Wachters, A. J. *J. Chem. Phys.* **1970**, *52*, 1033.
(54) Hay, P. J.; Wadt, W. R. *J. Chem. Phys.* **1985**, *82*, 284.
(55) Dunning, T. H.; Hay, P. J. In *Methods of Electronic Structure Theory*; Schäfer, H. F.; Ed.; Plenum Press: New York, 1977; Chapter 1.
(56) Møller, C.; Plesset, M. S. *Phys. Rev.* **1934**, *46*, 618.
(57) Schmidt, M. W.; Baldridge, K. K.; Jensen, J. H.; Koseki, S.; Gordon, M. S.; Nguyen, K. A.; Windus, T. L.; Elbert, S. T. *Quantum Chem. Prog. Exch. Bull.*, **1990**, *10*, 52.
(58) Gaussian 92, Revision C. Frisch, M. J.; Trucks, G. W.; Head-Gordon, M.; Gill, P. M. W.; Wong, M. W.; Foresman, J. B.; Johnson, B. G.; Schlegel, H. B.; Robb, M. A.; Replogle, E. S.; Gomperts, R.; Andres, J. L.; Raghavachari, K.; Binkley, J. S.; Gonzalez, C.; Martin, R. L.; Fox, D. J.; Defrees, D. J.; Baker, J.; Stewart, J. J. P.; Pople, J. A. Gaussian, Inc., Pittsburgh PA, 1992.
(59) GAMFORCE is written by Ø. Bache, Institute of Inorganic Chemistry, NTH, Trondheim, Norway, 1990.
(60) Sundius, T. *J. Mol. Struct.* **1990**, *218*, 321.